water

MDPI

Article

Analysis of Agricultural Drought Using Remotely Sensed Evapotranspiration in a Data-Scarce Catchment

Frank Joseph Wambura [1] and Ottfried Dietrich [2,*]

[1] Department of Urban and Regional Planning, Ardhi University, P.O. Box 35176, Dar es Salaam, Tanzania; frank.wambura@aru.ac.tz or wamburafj@gmail.com

[2] Leibniz Centre for Agricultural Landscape Research (ZALF) e. V., 15374 Müncheberg, Germany

* Correspondence: odietrich@zalf.de; Tel.: +49-33432-82305

Received: 21 February 2020; Accepted: 30 March 2020; Published: 1 April 2020



Abstract: Understanding spatial drought characteristics is vital for planning adaptation and mitigation measures in river catchments. In many parts of the world, spatial drought information is not available due to lack of adequate evenly distributed data for spatial drought analyses. This study elucidates a spatial drought analysis in a data-scarce tropical catchment using remote sensing actual evapotranspiration (ET) and potential evapotranspiration (PET) data. Firstly, the time series of 690 images of remotely sensed ET and PET between the years 2000 and 2014 were spatially analyzed using the evapotranspiration deficit index (ETDI) approach to obtain ETDIs in the Kilombero River catchment (Tanzania). Then, spatio-temporal patterns of ETDIs were used to characterize drought frequency, total drought durations, total drought severity, and drought intensity. The frequency, durations, severity, and intensity of drought increased from the year 2000 towards 2014, causing substantial drought changes in the catchment. However, drought intensity revealed that those changes were mainly from no drought and mild drought to moderate drought. Between the years 2000 and 2014, no-drought areas and mild drought areas declined from 10% to 0% and from 42% to 19%, respectively, whereas moderate drought areas increased from 47% to 81% of the catchment size. Those changes of drought conditions were partly attributed to anthropogenic land cover change, especially in the southwest grasslands, and were partly attributed to meteorological factors in other parts of the catchment. This information is crucial for further land cover change and climate change investigations, as well as planning water and land resources in the Kilombero River catchment. Moreover, the study also demonstrates the potential of using publicly available remote sensing ET products and the ETDI approach for spatially characterizing drought in ungauged regions.

Keywords: drought frequency; drought intensity; evapotranspiration deficit index; Kilombero; total drought durations; total drought severity; water stress

1. Introduction

Drought is an environmental disaster that has harsh and long-lasting impacts on natural and human systems. Drought impacts include humanitarian disasters, economic losses, and stresses on various elements of the environment [1]. Drought is usually characterized using its frequency (how often a drought occurs), duration (the length of a drought), severity (the strength of a drought), and intensity (degree of precipitation shortfall) [2,3]. Information about drought frequency, duration, severity, and intensity is very important in planning adaptation and mitigation measures for reducing drought impacts. In many parts of the world, the coverage of this information is not known or properly documentend because of data scarcity. As a result, many drought analysis studies, especially in

sub-Saharan Africa, have been using point data, particularly observed rainfall datasets [4,5]. This has been causing inadequate information about drought coverage, thus affecting the livelihood of many people in this region. For example, in the year 2009, Ethiopia was hit by severe drought leading to 6 million people in need of food [6,7]. Between the years 2016 and 2017, Kenya experienced drought conditions that also led to over 3 million people in need of food [8]. In Tanzania, the coastal zone experienced relatively high drought duration, severity, and intensity with more frequent extreme events after the year 2000 than before [5].

Because any meteorological phenomenon has subsequent impacts on hydrology and vegetation, drought, therefore, is usually divided into three main operation-based types [9]. These are meteorological drought, hydrological drought, and agricultural drought [3,4,10–13]. However, this study focused only on agricultural drought because it accomodates both meteorological and anthropogenic effects on water resources, especially in sub-Saharan Africa [7,8]. Because agricultural drought is a condition of insufficient soil moisture mainly due to a shortage of precipitation over some time period [14], its analysis is therefore based on monitoring water balance parameters and their subsequent deficit in the event of drought [9]. Several indices have been developed to calculate agricultural drought using various water balance parameters. Most of these indices use parameters such as precipitation, temperature, actual evapotranspiration (ET), and potential evapotranspiration (PET), together with soil physical properties, crop characteristics, and crop management practices, among others [1,9,15–19]. For a full discussion about these drought indices, including their strengths and weaknesses, see Sivakumar et al. [17] and Zargar et al. [9]. Due to data scarcity in many large catchments (>40,000 km^2) such as Kilombero river catchment in Tanzania [20,21] and the need for less data-intensive approaches, this study focused on agricultural drought indices that use a few types of data. Some of these indices are Drought Severity Index (DSI) [22], Soil Moisture Deficit Index (SMDI), and Evapotranspiration Deficit Index (ETDI) [23].

The DSI uses remotely sensed ET, PET, and normalized difference vegetation index (NDVI) products for estimation of drought severity [22], however, its formulae use mean as a mid-point and thus can be affected by outliers or single dominant event, whereas as SMDI and ETDI formulae use median as a mid-point [23]. The SMDI uses soil moisture for indicating long-term drought conditions [23], whereas ETDI uses ET and PET for indicating short-term drought conditions [23]. Both SMDI and ETDI can be scaled between −2 and +2 to compare with Standardized Precipitation Index values [24–29] or between −4 and +4 to compare with Palmer Drought Severity Index values [23,30]. This study focused on the use of ETDI for estimating short-term drought because it reflects both soil moisture state and plant health. Moreover, ET accounts for the largest water loss in river catchments.

Because many regions of the world lack sufficiently spatially distributed measured ET and PET data, currently, spatio-temporal analysis of ETDI have been using simulated ET and PET from hydrological models [4,23]. For example Narasimhan and Srinivasan [23] used ET and PET from a hydrological model with spatial resolution of 16 km^2. That coarse resolution neglects spatial variability of ET and PET, which is very important in large river catchments, especially in tropical regions [31,32]. Therefore, due to limited spatial distribution of computational units in distributed hydrological models, remote sensing products are the only viable data for mapping ET and PET in large catchments. Nowadays ET and PET from remote sensing products are freely available at moderate to high spatio-temporal resolution [33], for example, from the Moderate Resolution Imaging Spectroradiometer (MODIS) imagery program [34]. Moreover, remote sensing-based indices have already been used to monitor general vegetation state, vegetation health, and drought—these include DSI, NDVI, Enhanced Vegetation Index, Temperature Condition Index, and Normalized Difference Water Index [9,17,22].

The objective of this study was to use MODIS ET and MODIS PET to analyze spatio-temporal drought in the Kilombero catchment in Tanzania. Therefore, this study demonstrated spatio-temporal estimation of ETDI using readily available remote sensing products in a data-scarce catchment.

Moreover, the study also demonstrated spatio-temporal evaluations of drought frequency, durations, severity, and intensity from remote sensing-based ETDI.

2. Materials and Methods

2.1. Case Study

The Kilombero River catchment is located between 7°39′ S–10°2′ S and 34°33′ E–37°20′ E in south-central Tanzania (Figure 1). The catchment is part of the mighty Rufiji River basin, the largest river basin in Tanzania. The catchment encompasses the Kilombero valley and its surrounding mountains including the Mahenge highlands. The catchment is surrounded by the Mbarika Mountains in the southeast and the Udzungwa Mountains in the northwest.

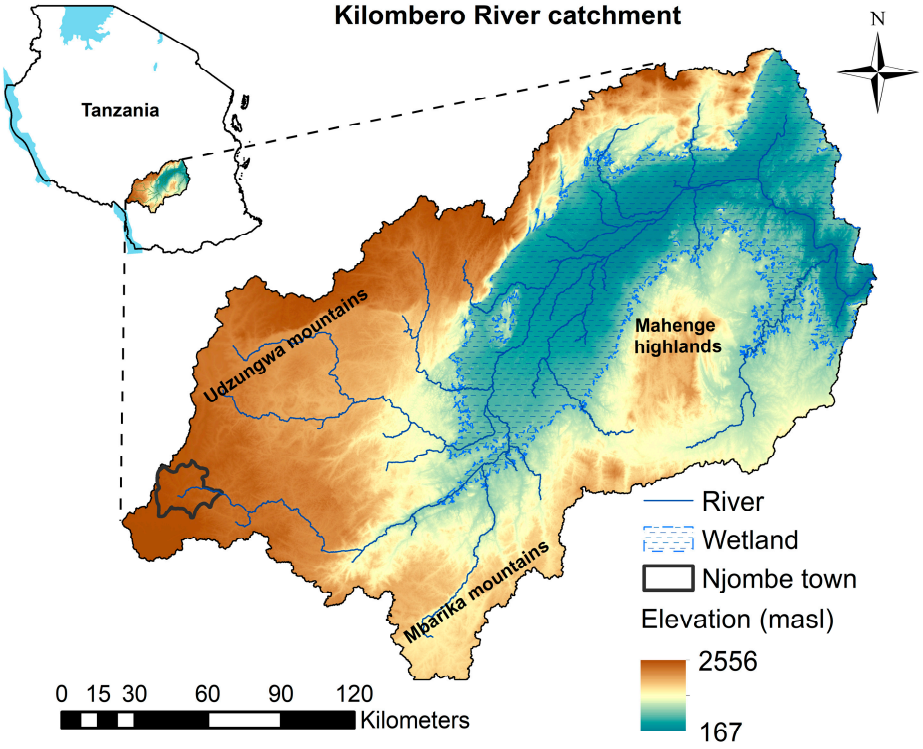


Figure 1. Kilombero River catchment (elevation: [35]).

The catchment area is approximately 40,390 km^2 and its elevation ranges between 167 and 2556 meters above sea level (Figure 1) [35]. The main river in the catchment is the Kilombero River, which flows towards the northeast. The catchment contributes about 62% of the annual runoff volume in the mighty Rufiji River basin [36]. A prominent hydrological feature in the catchment is the seasonal wetland at the Kilombero valley that has been designated as a Ramsar site [20,21,37]. The main land covers in the Kilombero catchment are savannas, evergreen forests, grasslands, and woody savannas (Figure 2) [38], and on average, these land covers constitute 47%, 14%, 14%, and 13% of the catchment area, respectively (Figure 2 and Table 1). Woody savannas are found in the south and southeast of the catchment, whereas grasslands are localized in the southwest of the catchment and along the Ramsar site. Evergreen forests are scattered in the northwest and south of the catchment.

The Kilombero River catchment is characterized by a sub-humid tropical climate, with a predominantly unimodal rainfall pattern from November to May [20]. The average annual rainfall in the catchment ranges between 1100 and 2100 mm [36]. The eastern Mahenge highlands, the Udzungwa Mountains, and low altitude southwest plains receive high amounts of rainfall, between 1500 and 2100 mm per annum. The Kilombero Valley experiences annual rainfall between 1200 and 1400 mm [36].

The distinct rainy season in the catchment is between December and April, and the distinct dry season is between June and October [20]. The June–September period usually has a monthly rainfall below 10 mm, except in the Udzungwa Mountains [21]. The annual mean temperature in the highlands and in the Kilombero Valley is around 17 °C and 24 °C, respectively. December and January are usually the hottest months, where day temperatures can exceed 19 °C in the mountains and 27 °C in the lowlands [36]. The coldest month is usually July, with temperatures around 14 °C and 21 °C in the highlands and lowlands, respectively. The average daily ET (derived from 8day MODIS ET data) in the catchment is about 3 mm.

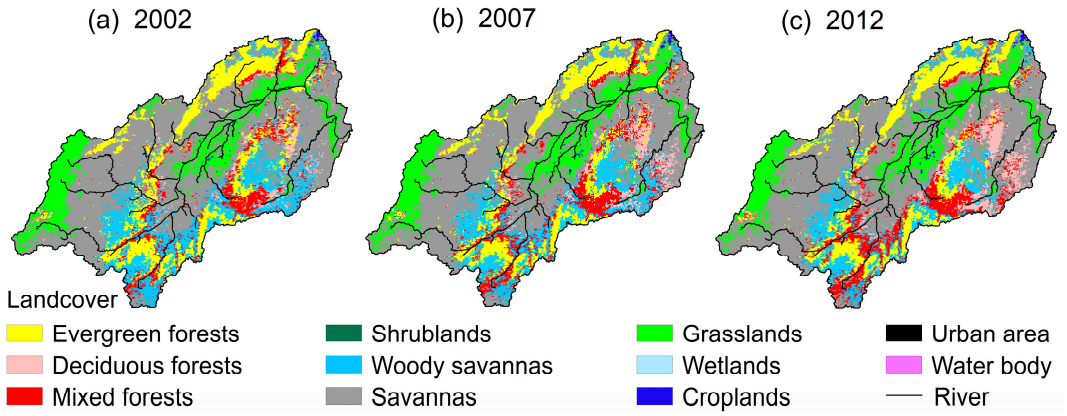


Figure 2. Moderate Resolution Imaging Spectroradiometer (MODIS) imagery program land cover classes in the Kilombero River catchment for the years 2002 (**a**), 2007 (**b**), and 2012 (**c**) [38].

Table 1. Moderate Resolution Imaging Spectroradiometer (MODIS) imagery program land covers in the Kilombero River catchment for the years 2002, 2007, and 2012 [38].

Land Cover (%)	2002	2007	2012
Evergreen forest	15	14	13
Deciduous forest	2	4	5
Woody savannas	14	13	11
Mixed forest	7	8	9
Savannas	47	47	48
Grasslands	14	14	14

The major anthropogenic activity in the Kilombero catchment is agriculture. Agricultural activities in the catchment include small-scale and large-scale farming, as well as pastoralism. Future plans in the catchment propose establishment of an agricultural growth corridor [39,40] in order to increase food production to match the rapid growth of human population in the region. With that magnitude of significance in food security in the region, the Kilombero River catchment requires sufficient information about drought frequency, durations, severity, and most importantly their spatial coverage.

2.2. Data Used

The MODIS product used in analyzing agricultural drought was MOD16A2 version 5, available at spatial and temporal resolutions of 1 km and 8 days, respectively [34]. A total of 690 MOD16A2 hierarchical data format (HDF) files were downloaded from the MODIS repository (http://files.ntsg.umt.edu/data/NTSG_Products/MOD16/, accessed on 15 October 2017). For MODIS products, an 8-day period is a unit of time similar to a week or a month. Therefore, the downloaded time series had 690 8-day periods.

The MOD16A2 files contain MODIS ET and MODIS PET datasets developed on the basis of the Penman–Monteith equation [34]. The 690 images of MODIS ET and 690 images of MODIS PET

(in the Geotiff format) covering the Kilombero catchment were extracted from the HDF files. Each image constituted 47,144 pixels covering the areas of the Kilombero River catchment. Therefore, there were 47,144-pixel time series of MODIS ET and 47,144-pixel time series of MODIS PET each with record length of 690 data points. The average cloud cover per MODIS image (estimated from 690 MODIS quality control images) was 14.5%. Pre-processing of the MODIS ET dataset for cloud masking was omitted because clouds neither often repeated on certain pixels nor were of large spatial extent per image [41]. Figure 3 represents patterns of average MODIS PET and MODIS ET in the Kilombero catchment.

Other subsidiary datasets used in this study included digital elevation model, land cover, and DSI data both for case study descriptions and interpretation of results. A digital elevation model with 90m resolution was downloaded from the Shuttle Radar Topography Mission database [35]. Land cover for the years 2002, 2007, and 2012 were downloaded from the MODIS land cover repository (https://e4ftl01.cr.usgs.gov/MOTA/, accessed on 26 July 2019) [38]. The DSI images for the years 2000, 2005, and 2010 were downloaded from the MODIS DSI repository (http://files.ntsg.umt.edu/data/NTSG_Products/DSI/, accessed on 07 July 2019) [22].

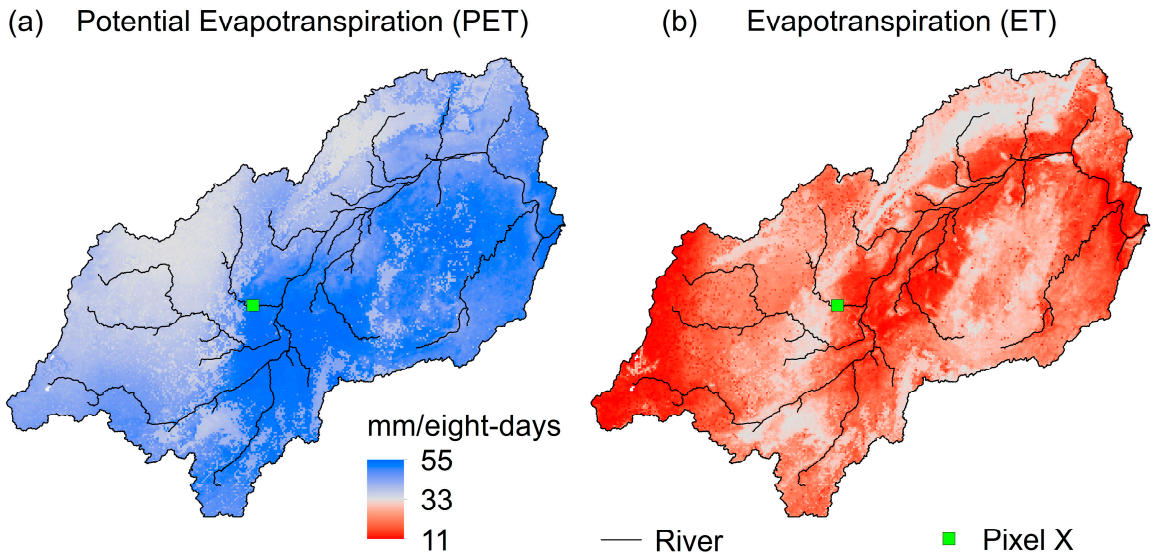


Figure 3. (**a**) 8-day average Moderate Resolution Imaging Spectroradiometer (MODIS) imagery program potential evapotranspiration (PET) (2000–2014), and (**b**) 8-day average MODIS evapotranspiration (2000–2014) in the Kilombero River catchment [34]. Pixel X shows the location of the timeseries used for illustration of drought analysis.

2.3. Methods

The approach used to analyze agricultural drought involved two steps, namely, estimation of ETDI and computation of drought characteristics. Estimation of ETDI used ET and PET to calculate consecutive 8-day periods of dry and wet conditions for each pixel in the Kilombero River catchment. Then, ETDI time series of pixels were used to identify drought events and calculate drought frequency, durations, severity, and intensity. These drought characteristics aimed at typifying the catchment drought conditions. The following sections describe in detail about estimation of ETDI.

2.3.1. Evapotranspiration of Deficit Index

The ETDI estimation used time series of MODIS ET and MODIS PET at a pixel level (Figure 4a–c). Firstly, water stress (WS) for each 8-day period in a year at a pixel level were computed using Equation (1) [4,23]. WS ranges from 1 (no ET) to 0 (ET is the same as PET).

$$WS_{(i,j,k,n)} = \frac{PET_{(i,j,k,n)} - ET_{(i,j,k,n)}}{PET_{(i,j,k,n)}} \quad (1)$$

where the subscripts i and j stand for x- and y-coordinates of a pixel, respectively. The subscript k represents an 8-day period in year n. Because there are about 46 8-day periods in a year, the subscript k ranges between 1 and 46 with a timestep of one 8-day period. The subscript n ranges between the years 2000 and 2014, with a timestep of 1 year.

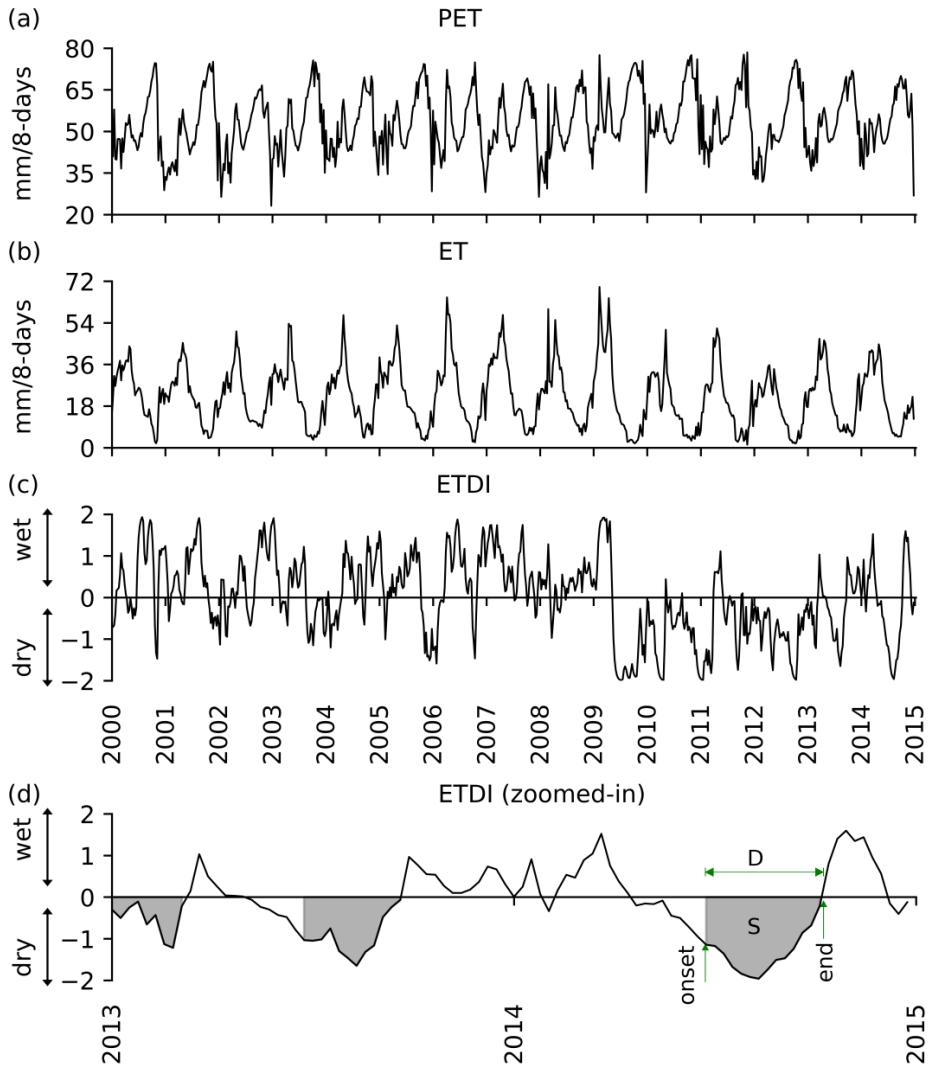


Figure 4. Graphical representation of data and drought analysis on the example of pixel X in Figure 2. (**a**) Potential evapotranspiration (PET). (**b**) Evapotranspiration (ET). (**c**) Evapotranspiration deficit index (ETDI). (**d**) Zoomed-in version of ETDI for illustrating onset and end of drought events (shaded regions), drought duration (D), and drought severity (S).

Then, the water stress anomaly (WSA) for each 8-day period in a year at a pixel level were also computed using Equation (2) [23].

$$WSA_{(i,j,k,n)} = \begin{cases} \frac{med\ WS_{(i,j,k)} - WS_{(i,j,k,n)}}{med\ WS_{(i,j,k)} - min\ WS_{(i,j,k)}} \times 100\%\ if\ WS_{(i,j,k,n)} \leq\ med\ WS_{(i,j,k)} \\ \frac{med\ WS_{(i,j,k)} - WS_{(i,j,k,n)}}{max\ WS_{(i,j,k)} - med\ WS_{(i,j,k)}} \times 100\%\ if\ WS_{(i,j,k,n)} > med\ WS_{(i,j,k)} \end{cases} \quad (2)$$

where med WS is the median water stress, min WS is the minimum water stress, and max WS is the maximum water stress for an 8-day period computed from all values of that period between the years 2000 and 2014. Median water stress removes seasonality [23]. WSA ranges from −100 to +100, indicating very dry to very wet conditions, respectively.

Because the focus of this study was on spatio-temporal estimation of ETDIs, the common and specific ETDI equation was used to estimate ETDIs. This equation states that the current ETDI is the sum of half of the previous ETDI and the current WSA (Equation (3)) [23]. The current WSA was divided by 100 to scale ETDI between −2 (very dry condition) and +2 (very wet condition) like the standard precipitation index [42], as shown in Table 2.

$$ETDI_{(i,j,t)} = 0.5\ ETDI_{(i,j,t-1)} + \frac{WSA_{(i,j,t)}}{100} \quad (3)$$

Here, an 8-day time step (k) and annual time step (n) variables were replaced with a continuous time step (t) variable. The subscript t ranges between 1 and 690 (record length) with a time step of 1 period. It was also considered that at initial condition (t = 1), the previous ETDI was equal to zero.

Table 2. Drought classification scheme based on Standard Precipitation Index [42].

Drought Intensity	Drought Category
Equal to 0.00	No drought
−0.01 to −0.99	Mild drought
−1.00 to −1.49	Moderate drought
−1.50 to −1.99	Severe drought
Equal to −2.00	Extreme drought

The WS, WSA, and ETDI equations were implemented in the Python programming environment (source codes are freely available upon request). After computation of ETDI time series for all pixels in the Kilombero River catchment, the time series were then used in estimation of drought characteristics.

2.3.2. Drought Characterization

The ETDIs of pixels in the Kilombero catchment for the period between the years 2000 and 2014 show negative and positive values which represent dry and wet conditions, respectively (see illustrations in Figure 4c–d). In this study, drought characterization focused on negative values of ETDIs. The start of a drought event was considered as a point in time when ETDI was less or equal to −1.0 (Figure 4d), and negative values continued for at least eight consecutive 8-day periods, that is, for approximately 2 months [42,43]. The ETDI value of −1.0 was selected as the starting-point because it indicates a deficit equivalent to unit standard deviation below normal or no drought condition (Table 2) [44]. The end of a drought event was considered as the time when ETDI returned to zero values (Figure 4d) [43,45]. The ETDI value of zero was selected as the end-point because usually after the start of a drought event any subsequent negative ETDI cumulatively contributes to the total drought condition.

Once the starts, ends, and number of drought events for a 5-year time series of each pixel were identified (as in Figure 4d), drought frequency (DF), total drought durations (TDD), total drought severity (TDS), and drought intensity (DI) were computed. DF is the number of drought events per

quinquennium. TDD is the total number of months from all drought events in a quinquennium [46]. Therefore, 8-day periods were converted into months (46 8-day periods are equivalent to 12 months). The TDS represents severity of all drought events occurring in a quinquennium. It was computed as the cumulative sum of ETDIs from TDD [5]. The DI was calculated as the ratio of TDS to TDD. The DF, TDD, TDS, and DI formulae for a 5-year time series of a pixel were implemented in the Python programming environment (source codes are freely available upon request). In order to monitor short period drought changes, drought characterization was performed for three quinquennia, namely, 2000–2004, 2005–2009, and 2010–2014 periods.

3. Results

3.1. Drought Characteristic: Frequency

The maps of DF in the Kilombero catchment show that the number of drought events in the three quinquennia ranged between 0 and 10 (Figure 5). The map of the first quinquennium shows that the area southwest of the catchment did not experience drought at all (Figure 5a). However, the largest part of the catchment experienced about 1 to 4 drought events (Figure 5a,b). During the second quinquennium, the largest part of the catchment experienced 1 to 3 drought events (Figure 5c,d). During this period, the largest part of the catchment experienced only two drought events (Figure 5d). There were also few spots of no drought events scattered across the catchment (Figure 5c). During the third quinquennium, the largest part of the catchment experienced about 3 to 6 drought events, although there were spots of 1 to 2 and 7 to 10 drought events (Figure 5e,f). Areas with no drought events in the first, second, and third quinquennia covered about 10%, 1%, and 0% of the catchment, respectively (Figure 5b,d,e).

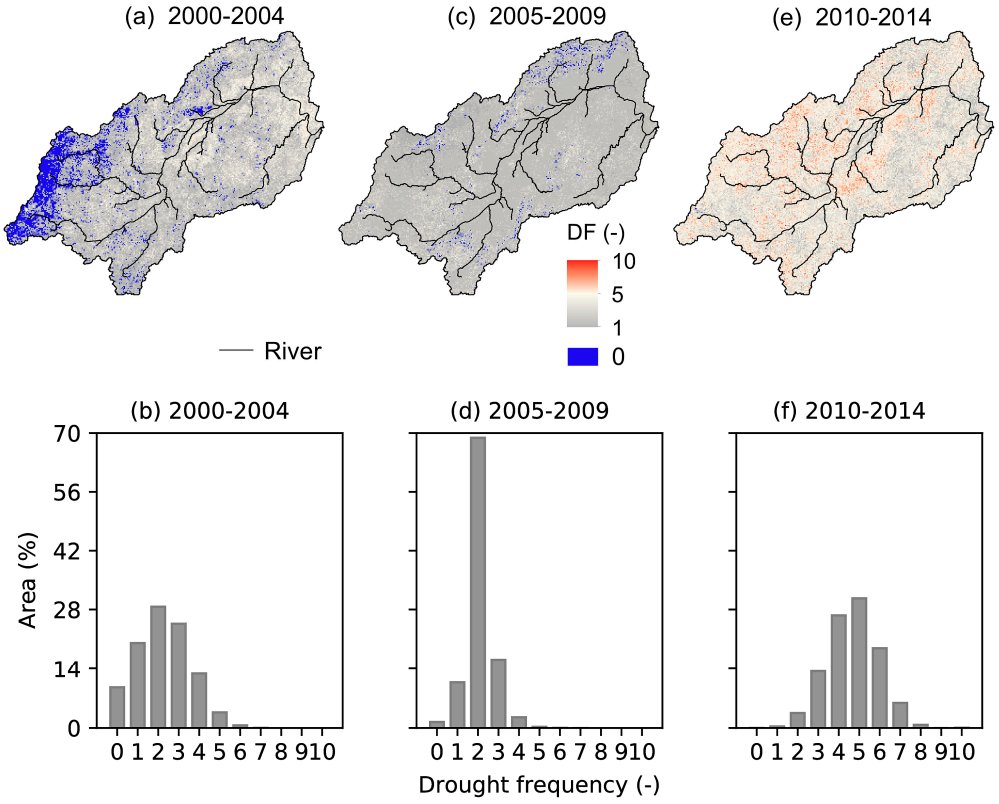


Figure 5. Map (**a**) and histogram (**b**) of drought frequency (DF) during the first quinquennium. Map (**c**) and histogram (**d**) of DF during the second quinquennium. Map (**e**) and histogram (**f**) of DF during the third quinquennium.

3.2. Drought Characteristic: Total Durations

During the first quinquennium, TDD ranged between 0 and 44 months. In this period, 81% of the catchment area had TDD between 2 and 15 months, whereas 10% of the catchment area did not experience drought at all (TDD = 0) especially in the southwestern part of the catchment (Figure 6a,b). During the second quinquennium, 92% of the catchment area also had TDD between 2 and 15 months, and the remaining area had few scattered spots of zero TDD (Figure 6c,d). During the third quinquennium, almost the entire catchment had lost zero TDD. In this period, 82% of the catchment area had TDD between 16 and 32 months. Moreover, 9% of the catchment area had scattered spots of TDD between 33 and 45 months especially in the southern part of the catchment and at the wetland (Figure 6e,f).

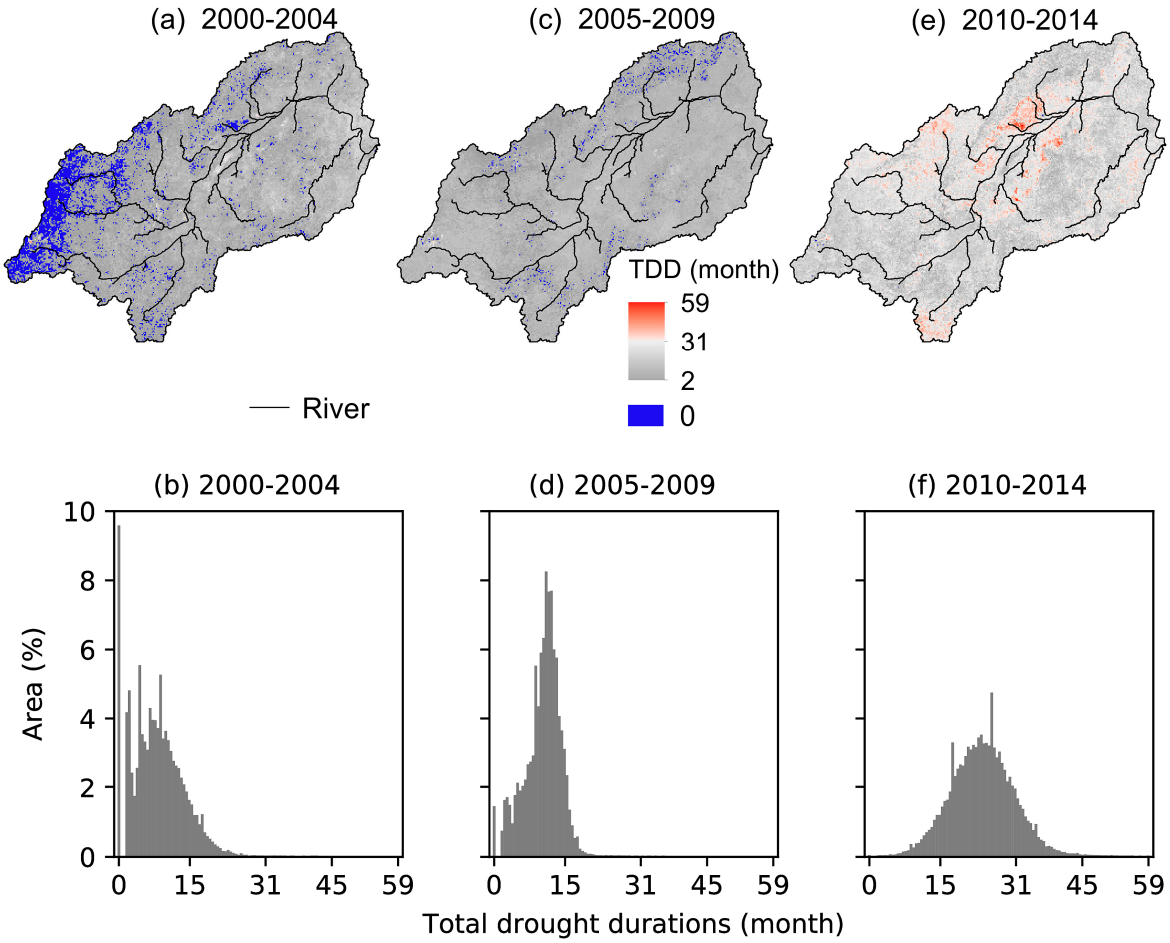


Figure 6. Map (**a**) and histogram (**b**) of total drought durations (TDD) during the first quinquennium. Map (**c**) and histogram (**d**) of TDD during the second quinquennium. Map (**e**) and histogram (**f**) of TDD during the third quinquennium.

3.3. Drought Characteristic: Total Severity

Like DF and TDD, the pattern of TDS also shows that the southwestern part of the catchment had no drought severity during the first quinquennium (cf. Figure 5a, Figure 6a, and Figure 7a). During this period, 10% of the catchment area experienced zero TDS, whereas 81% of the catchment area experienced TDS between −2 and −60. Moreover, the remaining part of the catchment experienced TDS mainly between −61 and −135 (Figure 7a,b). During the second quinquennium, areas experiencing zero TDS diminished to 1%, whereas an area experiencing TDS between −61 and −135 increased to 17% of the catchment area. In this period, 81% of the catchment area still experienced TDS between −2

and −60 (Figure 7c,d). Unlike the first and second quinquennia during the third quinquennium, 83% of the catchment area experienced TDS between −60 and −135. In this period, 8% of the catchment area experienced −2 and −60, whereas 9% of the catchment area experienced TDS beyond −135 (Figure 7e,f). TDS beyond −135 was somewhat experienced at the center and south of the catchment during the third quinquennium.

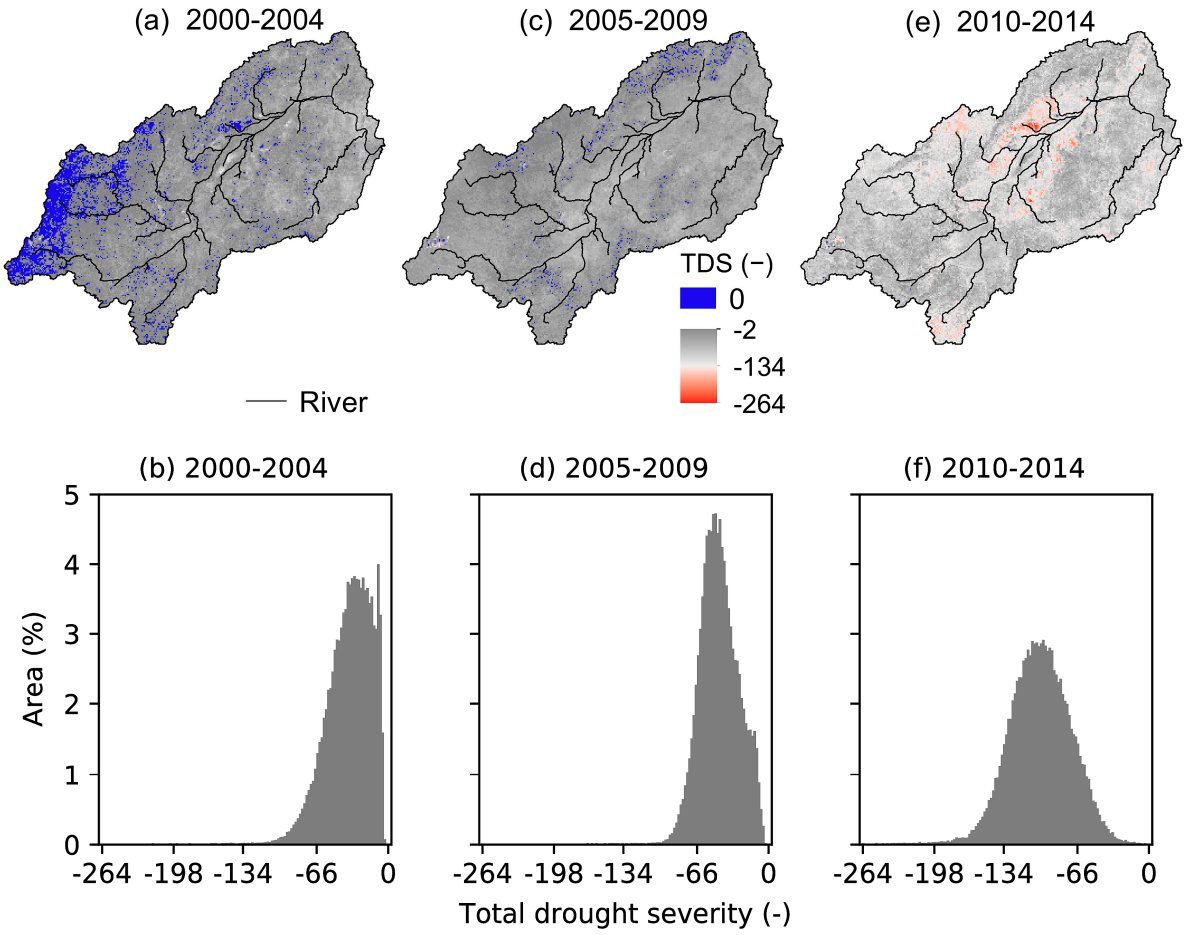


Figure 7. Map (**a**) and histogram (**b**) of total drought severity (TDS) during the first quinquennium. Map (**c**) and histogram (**d**) of TDS during the second quinquennium. Map (**e**) and histogram (**f**) of TDS during the third quinquennium.

3.4. Drought Characteristic: Intensity

During the first quinquennium, part of the catchment that exhibited zero DF, TDD, and TDS was also covered by no drought conditions (cf. Figure 5a, Figure 6a, Figure 7a, and Figure 8a). During this period, the no-drought area was about 10% of the catchment area (Figure 8 and Table 3). About 42% and 47% of the catchment area experienced mild drought and moderate drought, respectively. However, few spots of severe drought were also found in the south and northeast of the catchment during this period (Figure 8a). Figure 8b also shows that DI was almost equally distributed below and above the upper limit of moderate drought (DI equal to −1.00) during the first quinquennium.

Table 3. Spatial coverage of drought intensity categories in the Kilombero River catchment between the years 2001 and 2014.

Coverage (%)	2000–2004	2005–2009	2010–2014
No drought	10	1	0
Mild drought	42	33	19
Moderate drought	47	64	81
Severe drought	1	2	0
Extreme drought	0	0	0

During the second quinquennium, no drought and mild drought conditions substantially decreased to 1% and 33% of the catchment area, respectively, due to the increase of moderate drought to 64% and severe drought to 2% of the catchment area at the center towards northeast of the catchment (cf. Figure 8a,c and Table 3). This is also discernible in Figure 8d, where the DI distribution is slightly skewed towards lower values. Unlike the first and second quinquennia, during the third quinquennium moderate drought substantially increased to 81% of the catchment area at the expense of no drought, mild drought, and severe drought conditions (Figure 8e,f and Table 3). Mild drought substantially diminished to 19%, but tails of both no drought and severe drought conditions diminished completely (Figure 8f and Table 3).

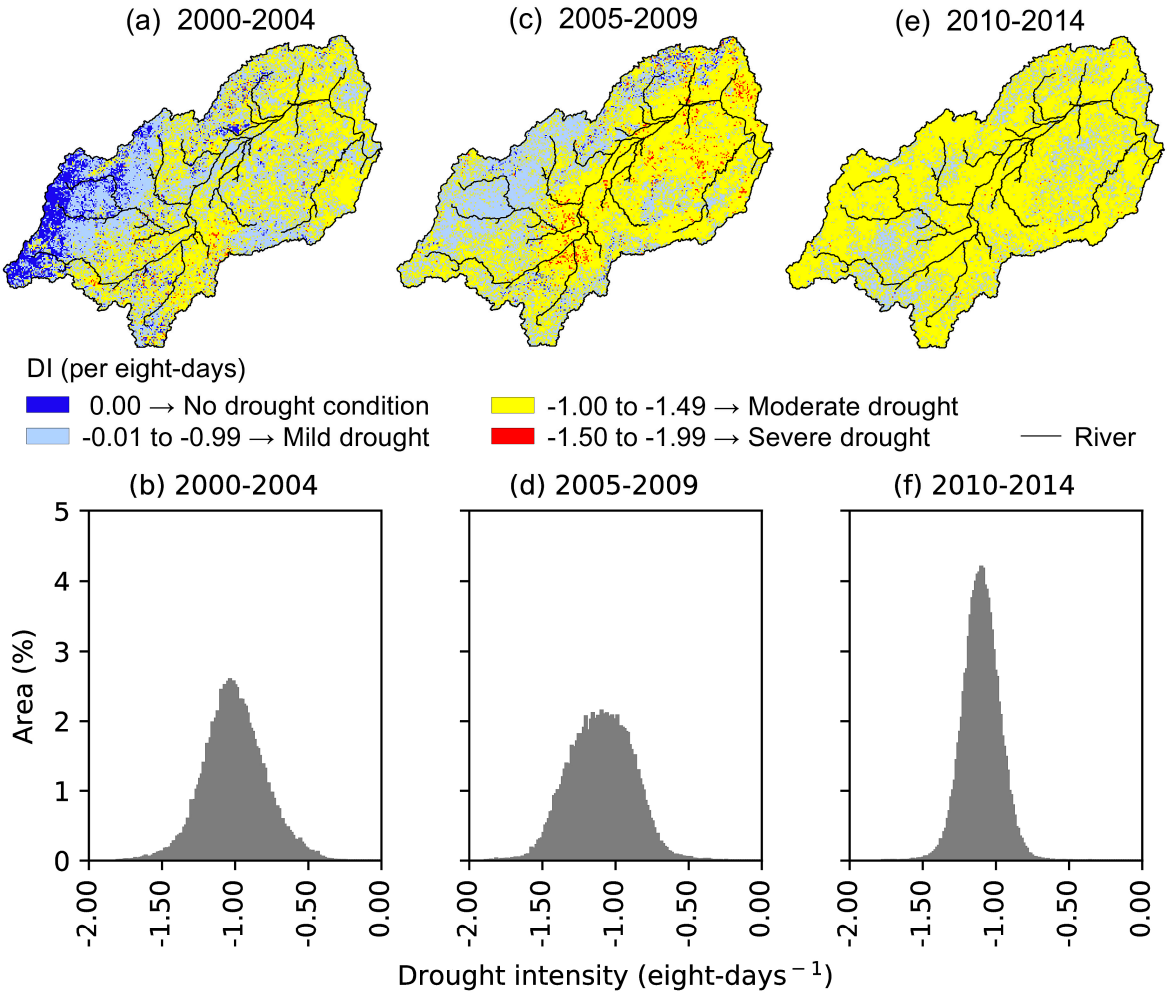


Figure 8. Map (**a**) and histogram (**b**) of drought intensity (DI) during the first quinquennium. Map (**c**) and histogram (**d**) of DI during the second quinquennium. Map (**e**) and histogram (**f**) of DI during the third quinquennium.

Most land covers in the catchment showed the increase of coverage of moderate drought and the decrease of coverage of no drought and mild drought during the three quinquennia (Table 4). For example, during the second and third quinquennia, parts of mixed forest, savannas, grasslands, and deciduous forests that were experiencing moderate drought increased. However, parts of woody savannas that were experiencing moderate drought did not change, although the one experienced mild drought decreased (Table 4). Parts of evergreen forest that were experiencing moderate drought decreased during the second quinquennium, but substantially increased during the third quinquennium (Table 4).

In comparison to the terrestrial DSI in the Kilombero River catchment, Mu et al. [22] also found that, since the year 2000, drought has been increasing whereas wet areas have been disappearing (cf. Figure 9). However, the patterns of wet condition during the year 2000 and no drought condition during the first quinquennium are not similar (cf. Figures 8 and 9). The former concentrated at the center along the river, whereas the latter was mainly in the southwest of the catchment.

Table 4. Drought intensity of land covers in the Kilombero River catchment. The first, second, and third quinquennia were compared against land covers for the years 2002, 2007, and 2012, respectively. N is no drought condition, Mi is mild drought, Mo is moderate drought, and S is severe drought.

Land Cover (%)	2000–2004				2004–2009				2010–2014			
	N	Mi	Mo	S	N	Mi	Mo	S	N	Mi	Mo	S
Evergreen forest	1	6	7	0	1	6	6	0	0	4	9	0
Deciduous forest	0	1	1	0	0	0	3	0	0	1	4	0
Woody savannas	0	6	8	0	0	4	8	0	0	3	8	0
Mixed forest	0	3	3	0	0	2	6	0	0	1	8	0
Savannas	4	22	22	0	0	16	29	1	0	8	40	0
Grasslands	4	5	5	0	0	4	10	0	0	1	13	0
Others	0	0	0	0	0	0	0	0	0	0	0	0

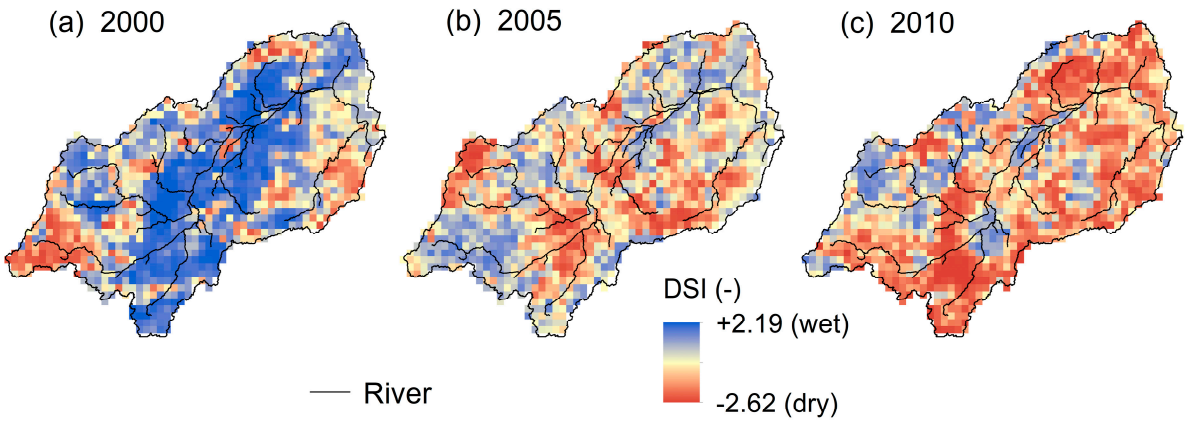


Figure 9. Annual terrestrial drought severity index (DSI) in the Kilombero River catchment for the years 2000 (**a**), 2005 (**b**), and 2010 (**c**) [22].

4. Discussion

4.1. General Approach

The objective of this study was to spatially characterize drought conditions in a data-scarce catchment for enhancing adaptation and mitigation measures. Therefore, information about drought frequency, duration, severity, and intensity was spatially or pixel-wise computed and presented. Unlike previous applications, which used lumped course resolution data from hydrological models to estimate drought severity [6,23], this study demonstrated the potential of ETDI in characterizing drought using

finer resolution remote sensing data. In this study, ETDIs were derived from MODIS PET and MODIS ET datasets.

Although there might be uncertainties associated with MODIS products [22,47], ETDI approach utilized relative values (i.e., ratios, Equations (1)–(3)) rather than absolute values. The latter require substantial ground-truth measurements for calibration or bias correction that are difficult to obtain, especially in a data-scarce region such as the Kilombero catchment [48]. Uncertainties due to ET estimation formula [34], image acquisition on MODIS satellites [49], cloud cover (≈15%), and geographical location might have effects on single values, however, systematic errors are known to have little effect on long-term anomalies [50]. Because the Kilombero catchment is in the equatorial region, these uncertainties were considered negligible. Moreover, some comparative studies in this region have shown that even absolute values of MODIS ET satisfactorily represent measured ET values [51,52]. These studies have shown that MODIS ET's spatial correlation ranges between 60% and 74% when compared with monthly measured or estimated ET in this region [51,52]. The following section describes findings on drought characteristics in the Kilombero River catchment.

4.2. Findings on Drought Characteristics

Like DF, TDD is not directly related to TDS; however, they all portray the presence of no-drought areas as well as drought-affected areas. DF maps revealed that about 88% of the Kilombero catchment experienced about one to five drought events in a 5-year period. This is equivalent to one drought event in any of the 5 years to one drought event in every year. Using standardized precipitation index in the east coast of Tanzania, Hassan et al. [5] also found that this region has recently been experiencing more than one drought episode per year. Because TDD shows an average of 2 to 6 months, and the dry period in the Kilombero catchment is usually between June and October [21,53–55], this implies that sometimes drought spells might coincide with dry periods (as shown in Figure 4d).

The disappearance of no-drought areas in the southwest of the catchment on the Udzungwa mountain ranges after the year 2004, as distinctively depicted by DF, TDD, TDS and DI, was caused by intensification of human activities in the grasslands around Njombe town. In this part of the catchment, drought condition might be anthropogenically driven. Although grassland did not change to other land covers, this area shifted from no drought condition to moderate drought condition, especially during the third quinquennium. This means that the growth of Njombe town affected patches of grassland but did not change the whole land cover completely. Other parts of the catchment also showed that patterns of drought events and intensity were not restricted to specific land covers. That is why similar drought patterns were experienced by woody savannas in the south and southeast, grasslands in the southwest and along the Ramsar site, evergreen forests in the northwest and south, and savannas in almost the entire catchment (Figures 2 and 8, Table 4). Moreover, land cover changes between consecutive quinquennia is negligibly small (≤3%; Table 1). This implies that drought in this catchment was not limited to anthropogenically-driven land cover changes.

Unlike other land covers, evergreen forests do not shed their leaves, even during the dry period [48,56]; therefore, changes in DF, TDD, TDS, and DI in these forests between the years 2000 and 2015 indicate meteorological effects. Msofe et al. [57] also found that annual rainfall in the Kilombero catchment between the years 1990 and 2017 has been significantly decreasing. Because rainfall in this catchment is linked to El Niño-Southern Oscillation and Indian Ocean Dipole [8], therefore, drought condition might also be linked to La Niña and negative Indian Ocean Dipole. However, it is difficult to separate these influences because they can strike at different times or at the same time.

The clear trend of the increase of areas experiencing moderate drought from the year 2000 towards 2014, as depicted by DI in the catchment, was also reported as DSI in the study by Mu et al. [22]. However, differences in the patterns of DI and DSI, especially at the center of the catchment, might be caused by differences in approach and data used [22,23]. The former used ET and PET data, whereas the latter used ET, PET, and NDVI. Moreover, DSI values are presented at very course resolution [22] as compared to DI.

5. Conclusions

The Kilombero River catchment is expected to undergo expansion and intensification of agricultural production in order to reduce food insecurity in the region. However, it still lacks enough evenly distributed measured hydrological data for guiding management plans. In order to enhance drought management plans in the catchment, this study focused on the analysis of drought characteristics. Drought frequency and durations showed that on average the largest part of the catchment experienced 1 to 5 drought event(s) per quinquennium. Moreover, DI showed the decrease of no-drought areas and mild drought areas, whereas moderate drought increased across the catchment. DI also showed that severe and extreme drought conditions between the year 2000 and 2014 were negligible. These changes are partly attributed to man-made land cover change, especially in the southwest areas around grassland of Njombe town and meteorological factors in other parts of the catchment. The increasing trend of moderate drought in the catchment is very important for planning intervention measures and uses of water and land resources in the catchment.

Apart from this, the study also demonstrated the usefulness of the ETDI method and drought characterization approach for disentangling anthropogenic effects from meteorological effects during drought condition in river catchments. Unlike other approaches that use many datasets, the ETDI approach uses only ET products. In addition, the study also provides evidence for a great potential of remote sensing ET products in estimating drought characteristics in data-scarce catchments. It is apparent that measured ET data would have produced more convincing findings. However, the extensive spatial drought information that can be estimated from remote sensing ET is very important for decision making in poorly gauged catchments around the world. Moreover, researchers can still improve estimates of drought information as more accurate and finer resolution remote sensing data becomes available.

Author Contributions: F.J.W. conceptualized this study, analyzed the data, interpreted the results, wrote the main text, and prepared tables and figures. O.D. also interpreted the results and gave important input to the manuscript. Both authors have read and agreed to the published version of the manuscript.

Funding: This research received no external funding.

Acknowledgments: The authors would like to thank the maintainers of the MODIS, SRTM, and FAO databases for providing MODIS ET, the digital elevation model, and land use data, respectively.

Conflicts of Interest: The authors declare no conflict of interest.

References

1. Touma, D.; Ashfaq, M.; Nayak, M.A.; Kao, S.-C.; Diffenbaugh, N.S. A multi-model and multi-index evaluation of drought characteristics in the 21st century. *J. Hydrol.* **2015**, *526*, 196–207. [CrossRef]
2. Van Loon, A.F.; Laaha, G. Hydrological drought severity explained by climate and catchment characteristics. *J. Hydrol.* **2015**, *526*, 3–14. [CrossRef]
3. Wilhite, D.A. Drought as a natural hazard: Concepts and definitions. In *Drought: A Global Assessment. Wilhite*; Routledge: London, UK, 2000; pp. 3–18.
4. Bayissa, Y.; Maskey, S.; Tadesse, T.; van Andel, S.; Moges, S.; van Griensven, A.; Solomatine, D. Comparison of the Performance of Six Drought Indices in Characterizing Historical Drought for the Upper Blue Nile Basin, Ethiopia. *Geosciences* **2018**, *8*, 81. [CrossRef]
5. Hassan, I.H.; Mdemu, M.V.; Shemdoe, R.S.; Stordal, F. Drought pattern along the coastal forest zone of Tanzania. *Atmos. Clim. Sci.* **2014**, *4*, 369–384. [CrossRef]
6. Bayissa, Y.A.; Moges, S.A.; Xuan, Y.; Van Andel, S.J.; Maskey, S.; Solomatine, D.P.; Griensven, A.V.; Tadesse, T. Spatio-temporal assessment of meteorological drought under the influence of varying record length: The case of Upper Blue Nile Basin, Ethiopia. *Hydrol. Sci. J.* **2015**, *60*, 1927–1942. [CrossRef]
7. Viste, E.; Korecha, D.; Sorteberg, A. Recent drought and precipitation tendencies in Ethiopia. *Theor. Appl. Climatol.* **2013**, *112*, 535–551. [CrossRef]
8. Peter, U.; Sjoukje, P.; Sarah, K.; Kasturi, S.; Joyce, K.; Emmah, M.; Jan, V.O.G.; Roop, S.; Julie, A.; Eddie, J.; et al. Attributing drivers of the 2016 Kenyan drought. *Int. J. Climatol.* **2018**, *38*, e554–e568. [CrossRef]

9. Zargar, A.; Sadiq, R.; Naser, B.; Khan, F.I. A review of drought indices. *Environ. Rev.* **2011**, *19*, 333–349. [CrossRef]
10. Wilhite, D.A.; Svoboda, M.D.; Hayes, M.J. Understanding the complex impacts of drought: A key to enhancing drought mitigation and preparedness. *Water Resour. Manag.* **2007**, *21*, 763–774. [CrossRef]
11. Ali, M.; Omid, M.; Amir, A. A hybrid framework for assessing socioeconomic drought: Linking climate variability, local resilience, and demand. *J. Geophys. Res. Atmos.* **2015**, *120*, 7520–7533. [CrossRef]
12. Ziolkowska, J. Socio-Economic Implications of Drought in the Agricultural Sector and the State Economy. *Economies* **2016**, *4*, 19. [CrossRef]
13. Mishra, A.K.; Singh, V.P. A review of drought concepts. *J. Hydrol.* **2010**, *391*, 202–216. [CrossRef]
14. Huang, Y.; Liu, X.; Shen, Y.; Jin, J. Assessment of Agricultural Drought Indicators Impact on Soybean Crop Yield: A Case Study in Iowa, USA. In Proceedings of the 2014 The Third International Conference on Agro-Geoinformatics, Beijing, China, 11–14 August 2014; pp. 1–6.
15. Hao, Z.; Singh, V.P. Drought characterization from a multivariate perspective: A review. *J. Hydrol.* **2015**, *527*, 668–678. [CrossRef]
16. Törnros, T.; Menzel, L. Addressing drought conditions under current and future climates in the Jordan River region. *Hydrol. Earth Syst. Sci.* **2014**, *18*, 305–318. [CrossRef]
17. Sivakumar, M.V.K.; Motha, R.P.; Wilhite, D.A.; Wood, D.A. Agricultural Drought Indices. In *Proceedings of the WMO/UNISDR Expert Group Meeting on Agricultural Drought Indices, Murcia, Spain, 2–4 June 2010*; AGM-11, WMO/TD No. 1572; WAOB-2011; World Meteorological Organization: Geneva, Switzerland, 2011; p. 197.
18. Martínez-Fernández, J.; González-Zamora, A.; Sánchez, N.; Gumuzzio, A. A soil water based index as a suitable agricultural drought indicator. *J. Hydrol.* **2015**, *522*, 265–273. [CrossRef]
19. Yang, H.; Wang, H.; Fu, G.; Yan, H.; Zhao, P.; Ma, M. A modified soil water deficit index (MSWDI) for agricultural drought monitoring: Case study of Songnen Plain, China. *Agric. Water Manag.* **2017**, *194*, 125–138. [CrossRef]
20. Koutsouris, A.J.; Lyon, S.W. Advancing understanding in data-limited conditions: Estimating contributions to streamflow across Tanzania's rapidly developing Kilombero Valley. *Hydrol. Sci. J.* **2018**, *63*, 197–209. [CrossRef]
21. Näschen, K.; Diekkrüger, B.; Leemhuis, C.; Steinbach, S.; Seregina, L.; Thonfeld, F.; van der Linden, R. Hydrological Modeling in Data-Scarce Catchments: The Kilombero Floodplain in Tanzania. *Water* **2018**, *10*, 599. [CrossRef]
22. Mu, Q.; Zhao, M.; Kimball, J.S.; McDowell, N.G.; Running, S.W. A Remotely Sensed Global Terrestrial Drought Severity Index. *Bull. Am. Meteorol. Soc.* **2013**, *94*, 83–98. [CrossRef]
23. Narasimhan, B.; Srinivasan, R. Development and evaluation of Soil Moisture Deficit Index (SMDI) and Evapotranspiration Deficit Index (ETDI) for agricultural drought monitoring. *Agric. For. Meteorol.* **2005**, *133*, 69–88. [CrossRef]
24. Guenang, G.M.; Kamga, F.M. Computation of the Standardized Precipitation Index (SPI) and Its Use to Assess Drought Occurrences in Cameroon over Recent Decades. *J. Appl. Meteorol. Climatol.* **2014**, *53*, 2310–2324. [CrossRef]
25. Šebenik, U.; Brilly, M.; Šraj, M. Drought Analysis Using the Standardized Precipitation Index (SPI). *Acta Geogr. Slov.* **2017**, *57*. [CrossRef]
26. Shah, R.; Bharadiya, N.; Manekar, V. Drought Index Computation Using Standardized Precipitation Index (SPI) Method For Surat District, Gujarat. *Aquat. Procedia* **2015**, *4*, 1243–1249. [CrossRef]
27. Pramudya, Y.; Onishi, T. Assessment of the Standardized Precipitation Index (SPI) in Tegal City, Central Java, Indonesia. *IOP Conf. Ser. Earth Environ. Sci.* **2018**, *129*, 012019. [CrossRef]
28. Li, J.Z.; Wang, Y.X.; Li, S.F.; Hu, R. A Nonstationary Standardized Precipitation Index incorporating climate indices as covariates. *J. Geophys. Res. Atmos.* **2015**, *120*, 12082–12095. [CrossRef]
29. Trambauer, P.; Maskey, S.; Werner, M.; Pappenberger, F.; van Beek, L.P.H.; Uhlenbrook, S. Identification and simulation of space–time variability of past hydrological drought events in the Limpopo River basin, southern Africa. *Hydrol. Earth Syst. Sci.* **2014**, *18*, 2925–2942. [CrossRef]
30. John, J.; Debra, P.; Lyons, D.L.; George, H. A tool for calculating the Palmer drought indices. *Water Resour. Res.* **2013**, *49*, 6086–6089. [CrossRef]

31. Wambura, F.J.; Dietrich, O.; Lischeid, G. Improving a distributed hydrological model using evapotranspiration-related boundary conditions as additional constraints in a data-scarce river basin. *Hydrol. Process.* **2018**, *32*, 759–775. [CrossRef]
32. Wambura, F.J.; Dietrich, O.; Graef, F. Analysis of infield rainwater harvesting and land use change impacts on the hydrologic cycle in the Wami River basin. *Agric. Water Manag.* **2018**, *203*, 124–137. [CrossRef]
33. Wang, L.; Wang, Y.; Xin, J.; Li, Z.; Wang, X. Assessment and comparison of three years of Terra and Aqua MODIS Aerosol Optical Depth Retrieval (C005) in Chinese terrestrial regions. *Atmos. Res.* **2010**, *97*, 229–240. [CrossRef]
34. Mu, Q.; Zhao, M.; Running, S.W. Improvements to a MODIS global terrestrial evapotranspiration algorithm. *Remote Sens. Environ.* **2011**, *115*, 1781–1800. [CrossRef]
35. Jarvis, A.; Reuter, H.I.; Nelson, A.; Guevara, E. Hole-Filled SRTM for the Globe Version 4. 2008. Available online: http://srtm.csi.cgiar.org (accessed on 28 October 2017).
36. Wilson, E.; McInnes, R.; Mbaga, D.P.; Ouedraogo, P. *Ramsar Advisory Mission Report*; Ramsar Site No. 1173; Kilombero Valley, United Republic of Tanzania: Dar es Salaam, Tanzania, 2018.
37. Siima, S.; Munishi, P.; Ngaga, Y.; Navrud, S. Estimating direct use value of Kilombero Ramsar Site based on market price method. *Tanzan. J. For. Nat. Conserv.* **2012**, *81*, 133–146.
38. Friedl, M.A.; Sulla-Menashe, D.; Tan, B.; Schneider, A.; Ramankutty, N.; Sibley, A.; Huang, X. MODIS Collection 5 global land cover: Algorithm refinements and characterization of new datasets. *Remote Sens. Environ.* **2010**, *114*, 168–182. [CrossRef]
39. URT United Republic of Tanzania. *Southern Agricultural Growth Corridor of Tanzania (SAGCOT) Investment Project*; Prime Minister's Office: Dar es Salaam, Tanzania, 2016.
40. MLHHSD. *Ministry of Lands, Housing and Human Settlements Development: National Land Use Framework Plan 2009–2029 (NLUFP 2009–2029)*; MLHHSD: Dar es Salaam, Tanzania, 2009; p. 183.
41. Müller, B.; Bernhardt, M.; Schulz, K. Identification of catchment functional units by time series of thermal remote sensing images. *Hydrol. Earth Syst. Sci.* **2014**, *18*, 5345–5359. [CrossRef]
42. McKee, T.; Doesken, N.; Kleist, J. The relationship of drought frequency and duration to time scales. In Proceedings of the Eighth Conference on Applied Climatology, Anaheim, CA, USA, 17–22 January 1993; p. 14027580.
43. Brito, S.S.B.; Cunha, A.P.M.A.; Cunningham, C.C.; Alvalá, R.C.; Marengo, J.A.; Carvalho, M.A. Frequency, duration and severity of drought in the Semiarid Northeast Brazil region. *Int. J. Climatol.* **2018**, *38*, 517–529. [CrossRef]
44. Dayal, K.S.; Deo, R.C.; Apan, A.A. Investigating Drought Duration-Severity-Intensity Characteristics Using the Standardized Precipitation-Evapotranspiration Index: Case Studies in Drought-Prone Southeast Queensland. *J. Hydrol. Eng.* **2018**, *23*, 05017029. [CrossRef]
45. Spinoni, J.; Naumann, G.; Vogt, J.; Barbosa, P. European drought climatologies and trends based on a multi-indicator approach. *Glob. Planet. Chang.* **2015**, *127*, 50–57. [CrossRef]
46. Spinoni, J.; Naumann, G.; Carrao, H.; Barbosa, P.; Vogt, J. World drought frequency, duration, and severity for 1951–2010. *Int. J. Climatol.* **2014**, *34*, 2792–2804. [CrossRef]
47. Yang, Y.; Long, D.; Guan, H.; Liang, W.; Simmons, C.; Batelaan, O. Comparison of three dual-source remote sensing evapotranspiration models during the MUSOEXE-12 campaign: Revisit of model physics. *Water Resour. Res.* **2015**, *51*, 3145–3165. [CrossRef]
48. Wambura, F.J.; Dietrich, O.; Lischeid, G. Evaluation of Spatio-Temporal Patterns of Remotely Sensed Evapotranspiration to Infer Information about Hydrological Behaviour in a Data-Scarce Region. *Water* **2017**, *9*, 333. [CrossRef]
49. Duveiller, G.; Lopez-Lozano, R.; Cescatti, A. Exploiting the multi-angularity of the MODIS temporal signal to identify spatially homogeneous vegetation cover: A demonstration for agricultural monitoring applications. *Remote Sens. Environ.* **2015**, *166*, 61–77. [CrossRef]
50. Munch, Z.; Conrad, J.E.; Gibson, L.A.; Palmer, A.R.; Hughes, D. Satellite earth observation as a tool to conceptualize hydrogeological fluxes in the Sandveld, South Africa. *Hydrogeol. J.* **2013**, *21*, 1053–1070. [CrossRef]
51. Deus, D.; Gloaguen, R. Remote Sensing Analysis of Lake Dynamics in Semi-Arid Regions: Implication for Water Resource Management. Lake Manyara, East African Rift, Northern Tanzania. *Water* **2013**, *5*, 698–727. [CrossRef]

52. Kiptala, J.K.; Mohamed, Y.; Mul, M.L.; Van Der Zaag, P. Mapping evapotranspiration trends using MODIS and SEBAL model in a data scarce and heterogeneous landscape in Eastern Africa. *Water Resour. Res.* **2013**, *49*, 8495–8510. [CrossRef]
53. Haule, K.S.; Johnsen, F.H.; Maganga, S.L.S. Striving for sustainable wildlife management: The case of Kilombero Game Controlled Area, Tanzania. *J. Environ. Manag.* **2002**, *66*, 31–42. [CrossRef] [PubMed]
54. Kirimi, F.; Thiong'o, K.; Gabiri, G.; Diekkrüger, B.; Thonfeld, F. Assessing Seasonal Land Cover Dynamics in the Tropical Kilombero Floodplain of East Africa. *J. Appl. Remote Sens.* **2018**, *12*. [CrossRef]
55. Koutsouris, A.; Seibert, J.; Lyon, S. Utilization of Global Precipitation Datasets in Data Limited Regions: A Case Study of Kilombero Valley, Tanzania. *Atmosphere* **2017**, *8*, 246. [CrossRef]
56. Fjeldså, J.; Kiure, J.; Doggart, N.; Hansen, L.; Perkin, A. Distribution of highland forest birds across a potential dispersal barrier in the Eastern Arc Mountains of Tanzania. *Steenstrupia* **2010**, *32*, 1–43.
57. Msofe, N.K.; Sheng, L.; Lyimo, J. Land Use Change Trends and Their Driving Forces in the Kilombero Valley Floodplain, Southeastern Tanzania. *Sustainability* **2019**, *11*, 505. [CrossRef]



© 2020 by the authors. Licensee MDPI, Basel, Switzerland. This article is an open access article distributed under the terms and conditions of the Creative Commons Attribution (CC BY) license (http://creativecommons.org/licenses/by/4.0/).